



# Easily Prepared Titanium Phosphate-Based Composites for the Remediation of Synthetic and Real Wastewaters

Doaa M. EL-Mekkawi · Sahar A. Othman ·  
Rasha M. Abd El-Wahab · Mohamed M. Selim

Received: 2 July 2022 / Accepted: 21 March 2023 / Published online: 3 April 2023  
© The Author(s) 2023

**Abstract** This study explored the remediation of polluted synthetic and real wastewaters by titanium oxyhydroxide/titanium phosphate (TTP) and TTP/active carbon (TTPC) composites. TTP materials were synthesized in mild conditions by hydrolyzing  $\text{TiCl}_4$  in a basic medium followed by the reaction with phosphoric acid. Analyses revealed that TTP is a nano-sized low crystalline material (average diameter of TTP ~ 6 nm) composed of 38.38%  $\text{TiO}(\text{OH})_2$  and 59.89% titanium phosphate. The maximal removal capacities of TTP were achieved in the highly basic waters. They were measured to be 10.60 and 11.55 meq/g TTP with respect to Na and K ions, respectively. The removal capacities of the individual parts of TTP are estimated to be 7.68 and 3.83 meq/g for titanium oxyhydroxide and hydrogen titanium phosphate, respectively, with respect to K ion. At high pH values, all exchangeable protons in the hydrogen titanium phosphate and titanium oxyhydroxide participated in the removal processes. Data also revealed that supporting

TTP on activated carbon enhanced its removal efficiency. The exposed surface area of supported TTP sample increased against the targeted cations during the removal experiments. Finally, full analysis of withdrawn real wastewater samples was conducted before and after their treatment using TTP materials. Both TTP and TTPC showed satisfied performance toward the removal of various metal ions and even against organic pollutants.

**Keywords** Titanium phosphate composite · Wastewater treatment · Removal capacity · Rahawy drain

## 1 Introduction

Due to the conditions that Egypt is going through, which are related to shortage of water resources, the reuse of wastewater is gaining more attention as an effective strategy (Ibrahim et al., 2020; EL-Mekkawi et al., 2020; EL-Mekkawi et al., 2016). Metal contamination of soil and water is a critical environmental problem (Sebastian et al., 2019). Sodic soils reduce the productivity of arid and semiarid lands. The high level of sodium restricts the infiltration of water into the soil as well as the water availability to plants (Sebastian et al., 2019). The existing potassium and sodium ions in water are essential for cellular and electrical processes. Abnormal levels of these ions may raise the risk of heart arrhythmias, weaken health of bones, and

D. M. EL-Mekkawi (✉) · R. M. Abd El-Wahab ·  
M. M. Selim  
Physical Chemistry Department, National Research  
Centre, NRC, 33 EL Bohouth St., Dokki, Giza P.O. 12622,  
Egypt  
e-mail: doaa\_egypt@yahoo.com; dm.mohammed@nrc.  
sci.eg

S. A. Othman  
Central laboratory for environmental quality monitoring  
(CLEQM), National Water Research Center (NWRC),  
Qalyubia, Egypt

hypokalemia. Therefore, it is necessary to control the amount of sodium and potassium ions in irrigating and drinking water within their normal limits (Ahn et al., 2018).

Inorganic ion exchangers are a promising class of materials for the removal of these undesired metal cations (Zhang et al., 2017). The most important advantages of the ion exchange process are their fast kinetics, high removal capacity and its capability to sorb metal cations present in trace amounts (EL-Mekkawi, and Selim, 2014; EL-Mekkawi et al., 2016; Selim et al., 2017). Titanium phosphate (TP) ion exchanger is an insoluble acid salt of tetravalent titanium metal. The presence of two types of functional groups, Ti–OH and phosphoric acid groups, enables titanium phosphate materials to display amphoteric behavior (Zhang et al., 2017). The protons within the phosphate groups are mostly responsible for the ion exchange process.

TP exhibits various structures according to the type of linkage between oxygen in the phosphate groups and titanium. Amorphous, fibrous, layered  $\alpha$ -TP and  $\gamma$ -TP, or three-dimensional titanium phosphates are previously investigated structures (Alberti et al., 1996; Serre et al., 2012; Trublet et al., 2016). The preparation of TP mostly involves long procedures and harsh conditions such as high pressure and temperatures. These complicated conditions raise the energy consumption and the cost of the preparation processes. Various methods have been introduced in literature for the synthesis of titanium phosphates (TP). TP was mostly prepared through the reaction of phosphoric acid or phosphate salts with titanium (Tegehall, 1986) or titanium-based materials. These materials include titanium oxides (Bruque et al., 1995; Maslova et al., 2018), alkoxides (Liu et al., 2010; Guo, and Han, 2014; Guo et al., 2014), or salts such as  $\text{TiCl}_4$  (Onoda and Yamaguchi, 2012a; Onoda and Yamaguchi, 2012b; Onoda et al., 2021),  $\text{TiCl}_3$  (Bortun et al., 1995),  $\text{TiSO}_4$  (Onoda et al., 2014), and  $\text{TiOSO}_4$  (Maslova et al., 2008).

On the other hand, it has been previously revealed that transformation of the titanium phosphate materials from their proton to sodium forms cannot be fully accomplished (Qureshi and Varshney, 1991). This was attributed to the existence of different exchange units, geometry restriction and possible partial hydrolysis of the material.

Activate carbon is extensively utilized in the remediation of waters contaminated with organic and

inorganic pollutants (Velo-Gala et al., 2017; Botome' et al., 2017; Suhas et al., 2017; Filipe-Ribeiro et al., 2017, Zhang et al., 2017; Björklund and Li, 2017). Active carbon is characterized by its porous structure and high surface area. It is expected that the removal of metal ions from wastewaters by TTP will be enhanced when supported on active carbon due to the high exposed surface area of the formed composite.

EL-Rahawy drain is the major source of pollution for Rosetta Branch (one of two branches of River Nile on Mediterranean Sea). It is the end part of EL-Mhiet agricultural drain. EL-Rahawy receives combined discharges from the agricultural drainage system and the two-sewerage plant (Zenein and Abo-Rawwash). This highly polluted streams flow into Rosetta Branch from the west side about 9 km north of Delta Barrage. The discharge of EL-Rahawy drain ranged from 1.9 up to 2.8 million  $\text{m}^3/\text{day}$ . The drain contains significant amount of sodium, potassium, toxic heavy metals, and organic pollutants. The Rahawy drain is mostly a basic stream. Thus, the aim of this research is demonstrating adequate TP materials with high removal capacity to be utilized at such operating circumstances.

Taking into account the above, this article represents a simple preparation method of high removal capacity titanium phosphate composites under mild experimental conditions. The method involves the hydrolysis of  $\text{TiCl}_4$  in a basic medium followed by the reaction with phosphoric acid. The suitability of the remediation of polluted synthetic and real wastewaters by titanium oxyhydroxide/titanium phosphate (TTP) and TTP-active carbon (TTPC) composites has been explored. The synthesized materials were fully characterized by using x-ray fluorescence (XRF), x-ray diffraction (XRD), high-resolution transmission electron microscopy (HRTEM), Fourier transform infrared (FTIR), and thermo gravimetric analysis (TGA). Surface characterizations were also investigated by using  $\text{N}_2$  adsorption/desorption measurements. The sorption behavior of the synthesized TTP composites against metal cations particularly Na and K ions were thoroughly investigated.

## 2 Materials and Methods

Titanium tetrachloride ( $\text{TiCl}_4$ ) was purchased from Merck. Ammonium hydroxide solution ( $\text{NH}_4\text{OH}$ , 30%)

was purchased from Adwic, Egypt. Sodium nitrate ( $\text{NaNO}_3$ ) and potassium nitrate ( $\text{KNO}_3$ ) were purchased from GFS, CHEMICALS, USA. Phosphoric acid ( $\text{H}_3\text{PO}_4$ , 95%) was purchased from Lach-Ner, Czech. All chemicals and materials were used as received.

Real wastewater samples were collected from Rahawy drain as a real case study. The sample was collected from the point of discharge of the drain into Rosetta Branch. Sampling and preservation procedures were carried out according to Standard Method for Examination of Water and Wastewater (Standard methods for the examination of water and wastewater, 2017). Full analysis of the collected real wastewater was given in the results and discussion section.

## 2.1 Synthesis of Titanium Phosphate Materials

Titanium phosphate (TTP) materials were synthesized by hydrolyzing  $\text{TiCl}_4$  in a basic medium followed by the reaction with phosphoric acid. 88 ml of  $\text{TiCl}_4$  dissolved in HCl (24% w/v) was transferred drop wise to solution containing 145 ml of  $\text{NH}_4\text{OH}$  solution in the absence and presence of activated carbon under vigorous stirring. Upon the completion of the reaction, the formed white precipitate of titanium oxyhydroxide (supported or unsupported) was washed with distilled water to get rid of any chloride ions. Phosphoric acid was then added drop by drop to form titanium phosphate until pH became 3. The synthesized samples were then washed thoroughly by distilled water until pH reached constant value (approximately 4.5). All samples were then dried in an oven at 100 °C. The synthesized unsupported and supported titanium phosphate samples were coded TTP and TTPC, respectively. The ratio of TTP to active carbon in the prepared TTPC composite was adjusted at 1:5. Active carbon was purchased from Atlantic Industries company, Egypt. Full analyses of the active carbon were carried out according to American Society for Testing and Materials “ASTM” (1999). The physicochemical characteristics of the active carbon are summarized in Table 1

## 2.2 Characterization of Titanium Phosphate Materials

### 2.2.1 X-ray Diffraction Measurements

Crystallinity and chemical composition of TTP materials were investigated by x-ray diffraction

**Table 1** physicochemical characteristics of the active carbon

| Parameter                        | Results                                  |
|----------------------------------|--|
| Iodine number                    | 988 mg/g                                 |
| Moisture content                 | 5.5%                                     |
| Particle size distribution       | 2% > 3 mm<br>97.8% 2–3 mm<br>0.2% > 1 mm |
| Apparent density                 | 0.48 g/cm <sup>3</sup>                   |
| Hardness                         | 92%                                      |
| Total ash                        | 2.05%                                    |
| Total sulfides                   | 1.39 mg/kg                               |
| Abrasion number                  | 71%                                      |
| Water extractable substances     | 1.87%                                    |
| Polycyclic aromatic hydrocarbons | 0.0066 µg                                |
| Dechlorination half value length | 2.67 cm                                  |
| Wettability                      | 99.3%                                    |
| Uniformity coefficient           | 1.9                                      |
| Water soluble materials          | 0.85% w/w                                |
| Zn                               | 0.0019 mg/kg                             |
| Fe                               | 0.006 mg/kg                              |
| Ti                               | 0.066 mg/kg                              |
| P                                | 0.05 mg/kg                               |
| Cl                               | 0.044 mg/kg                              |
| Na                               | 0.03 mg/kg                               |
| Mg                               | 0.022 mg/kg                              |
| Al                               | 0.036 mg/kg                              |
| Si                               | 0.088 mg/kg                              |
| K                                | 0.011 mg/kg                              |

technique. The XRD diffractograms of the synthesized TTP materials were determined using a Bruker diffractometer (Bruker D8 advance target). Cu  $K\alpha$  radiation source with secondly monochromator ( $\lambda = 1.5405 \text{ \AA}$ ) at 40 kV and 40 mA was used and the scanning rate was adjusted at  $0.2 \text{ min}^{-1}$ .

### 2.2.2 Elemental Analysis

The chemical composition of the prepared TTP sample was determined through its elemental analysis by using x-ray fluorescence (XRF Axios, sequential WD-XRF spectrometer, PANalytical 2005, Netherland). Grinding, pressing, and bead preparation of the investigated samples were carried out by using automated integrated sample preparation units.

### 2.2.3 High-Resolution Transmission Electron Microscopy

The surface morphology of TTP materials were studied by high-resolution transmission electron microscope (HRTEM). HRTEM images were taken on JEOLTEM- 1230 at 200 k eV acceleration voltage and camera length 8–12 m. The samples were dispersed in distilled water followed by ultrasonic vibration for half an hour. A drop of the dispersed sample was placed onto a copper grid coated with a layer of amorphous carbon.

### 2.2.4 FTIR Analyses

The characteristic functional groups on TTP surface were identified by using Fourier-transform infrared spectroscopy (FTIR). The FTIR transmission spectrum of TTP in the range 4000–400  $\text{cm}^{-1}$  was measured using FTIR-ATR Bruker Vertex 80V (Germany) combined with platinum diamond ATR, with resolution 4  $\text{cm}^{-1}$  and refractive index 2.4. The spectrum was recorded in IR grade KBr at room temperature.

### 2.2.5 Thermogravimetric Analysis

Thermogravimetric analysis (TGA) was performed to study the thermal decomposition of TTP by Themesys one, thermal analyzer, France. TGA analysis was carried out according to ASTM E1131, ISO 11358. Heating rate was set at 10  $^{\circ}\text{C}$  per minute from room temperature to 1000  $^{\circ}\text{C}$  under nitrogen atmosphere.

### 2.2.6 Surface Characterization

The surface characteristics of TTP materials were determined from  $\text{N}_2$  adsorption-desorption isotherms measured with BELSORPmax (BEL JAPAN INC.) at  $-196^{\circ}\text{C}$ . Samples were degassed for 24 h at 80  $^{\circ}\text{C}$  before taking the measurements. The specific surface area of each sample was calculated by the Brunauer-Emmett-Teller (BET) equation, whereas the micropore/mesopore volume was measured using the t-plot method.

Non-local density functional theory (NLDFT) model was applied to determine the porosity of TTP samples.

## 2.3 Removal of Na and K Ions by TTP Materials

Removal of Na and K ions by TTP materials from water was conducted using the batch method. Batch experiments were carried out using certain weight of TTP samples suspended in a solutions containing metal ions of different concentrations (weight/volume = 1:10). All experiments were carried at room temperatures (25  $^{\circ}\text{C}$ ). The mixtures in the bottles were shaken for 120 min. After each experiment, TTP materials were filtered. The exact concentrations of the removed Na and K ions were estimated using Flame photometer 410 Sherwood.

The sorption of metal cations by TTP materials was described by the Langmuir Eq. (1) (Langmuir, 1918)

$$1/q_e = C_e/q_m b + 1/C_e q_m \quad (1)$$

where  $q_e$  (mg/100g) and  $C_e$  (mg/L) are the amounts of removed metal ions per 100 g of the investigated samples and remaining metal ions concentration in solution at equilibrium, respectively.  $q_m$  is the maximum amount of removed metal ions per 100 g of solid sample to form a complete monolayer on the surface at high  $C_e$ , and  $b$  is a constant related to the affinity of the binding sites (L/mg).

## 2.4 Determination of Ion-Exchange Capacity

The ion-exchange capacity of titanium phosphate was investigated by a simple back titration method (Maslova et al., 2012). TTP sample was treated with 0.5 M NaOH for 12 h (solid:liquid = 1:100). The solution was then filtrated and titrated with 0.1 M HCl (using phenol phthalene as indicator). The exchange capacity  $E$  (in meq/g) was then estimated using the Eq. (2):

$$E = \frac{V_{\text{HCl}} \times M_{\text{HCl}} \times V_{\text{solution}}}{V_{\text{aliquot}} \times M_{\text{sorbent}}} \quad (2)$$

The ion-exchange capacity was similarly investigated by using KOH and the results were compared to that obtained by using NaOH.

## 2.5 Real Wastewater Analysis

Inductively coupled plasma -optical emission spectrometry (ICP-OES) with Ultra Sonic Nebulizer (USN) with instrumental detection limit 10%, Perkin Elmer Optima 5300, USA, was used to determine heavy metals (Ba, Cd, Co, Cu, Fe, Mn, and Zn) in the real wastewater samples. Electrical conductivity (EC) and pH values were measured at 25°C as standard temperature using bench-top electric conductivity and pH meter, WTW Multi 9620IDS, serial No:19211274. Ammonia determined by Ammonia electrode Orion STAR A214 serial No: SnX4281. Calcium and magnesium hardness were determined as calcium carbonate and magnesium carbonate by applying a titrimetric method with ethylene diamine tetra acetic acid (EDTA). Sodium salt of EDTA forms a chelate of a soluble complex when added to the water sample (standard methods for the examination of water and wastewater, 2017).

## 3 Results and Discussion

### 3.1 Synthesis of Titanium Oxyhydroxide/Phosphate Composites

In this research, titanium phosphate (TTP) materials were synthesized by hydrolyzing  $\text{TiCl}_4$  using  $\text{NH}_4\text{OH}$  solution followed by the interaction of phosphoric acid as previously indicated in the experimental

section. The precipitation of  $\text{TiCl}_4$  into the highly dispersed oxyhydroxide gel allowed robust interaction between the gel and phosphoric acid to form tiny nano-sized titanium phosphate under mild conditions. The pH of the solution was followed up to minimize the excess of the unreacted phosphoric acid. The formed samples were then fully characterized and investigated for the removal of metal cations as described later.

### 3.2 Characterization of TTP Materials

The synthesized TTP and TTPC were characterized using XRD, XRF, HRTEM, FTIR, and TGA as well as the nitrogen adsorption/desorption analyses as discussed below.

#### 3.2.1 XRD Analysis

The x-ray diffractogram of TTP is illustrated in Fig. 1. TTP displayed no sharp diffraction peaks, only broad peaks at 10–70°, indicating its low degree of crystallinity. Similar x-ray diffractograms were previously introduced for amorphous TTP (Trublet et al., 2016; Maslova et al., 2008).

The XRD diffractogram (Fig. 2) of TTP treated at 1000 °C indicates the formation of a mixture of  $\text{TiO}_2$  and titanium oxide phosphate  $\text{Ti}_5\text{O}_4(\text{PO}_4)_4$  phases. The mixture is composed of 18% anatase, 24% rutile, and 58% titanium oxide phosphate phases. The data matched the standard XRD data in Joint Committee on

**Fig. 1** XRD diffractogram of the synthesized TTP

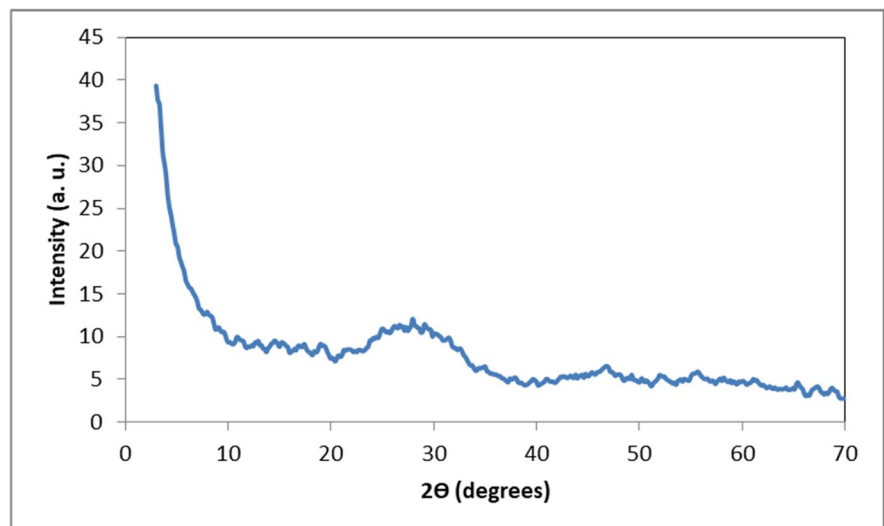


**Fig. 2** XRD diffractogram of the TTP after treatment at 1000 °C. A = anatase, R = rutile and P = titanium oxide phosphate

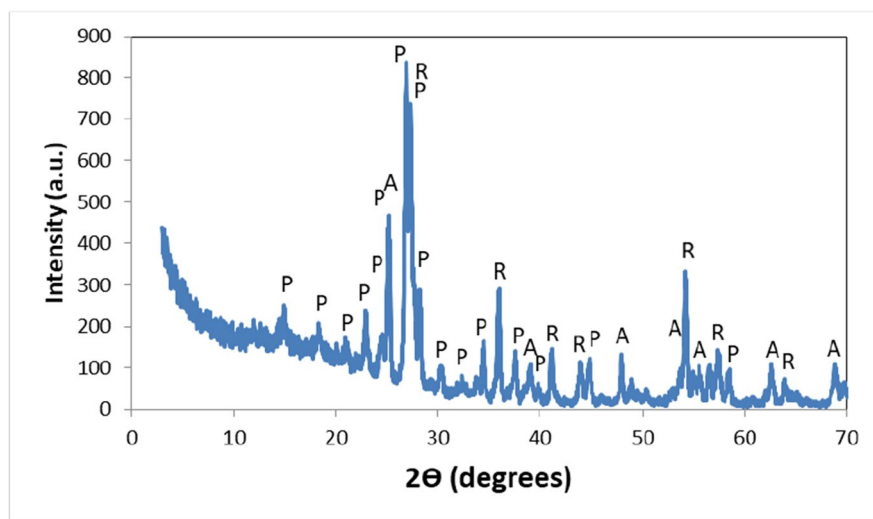


**Table 2** Chemical composition of TTP in % mass

| Oxide                         | Percentage |
|-------------------------------|------------|
| P <sub>2</sub> O <sub>5</sub> | 29.81      |
| TiO <sub>2</sub>              | 45.10      |
| Wt loss                       | 25.86      |

Powder Diffraction Standards (JCPDS); card files nos. 00-021-1276, 00-021-1272, and 01-087-0563 of rutile, anatase titania, and titanium oxide phosphate phases, respectively. This data indicates that the synthesized TTP sample composed of unreacted titanium oxyhydroxide and titanium phosphate.

### 3.2.2 Elemental Analysis

The chemical composition of the synthesized TTP sample was investigated by XRF measurement (see Table 2). As illustrated in Table 2, TTP composed of only Ti and P elements beside the weight loss (volatile water) which are the constituents of titanium oxyhydroxide and titanium phosphate phases. As indicated in Table 2, the TiO<sub>2</sub>:P<sub>2</sub>O<sub>5</sub> ratio in TTP sample was estimated to be 1.513 indicating the existence of TiO<sub>2</sub> as a separate phase as confirmed by XRD.

### 3.2.3 High-Resolution Transmission Electron Microscopy Analyses

Figure 3 illustrates high-resolution transmission electron microscopy (HRTEM) image of the synthesized TTP and TTPC. The obtained images in Fig. 3 confirm the formation of nano-sized TTP with narrow particle size distribution (average diameter of TTP ~ 6 nm). TTP is quasi-spherical in shape. Both of TTP and TTPC samples displayed layered structures. Figure 3b presents the diffraction pattern of the prepared sample indicating the low crystallinity of TTP. These results are in agreement with findings obtained by XRD. On the other side, increase in the amorphicity is observed in Fig. 3d due to the presence of active carbon.

### 3.2.4 FTIR Analysis

As shown in Fig. 4, FTIR spectrum of TTP displayed broad peak around 3400 cm<sup>-1</sup> which is attributed to overlapping asymmetric and symmetric OH stretching vibrations of surface water molecules and P-OH and Ti-OH groups. The peak at 1645 cm<sup>-1</sup> is assigned to the OH bending vibration of adsorbed water. The peaks in the region 1000–1060 cm<sup>-1</sup> can be referred to the Ti–O–P skeletal stretching vibrations (Janusz et al., 2019).

The band at 1045 cm<sup>-1</sup> is referred to the Ti–O–P stretching modes of HPO<sub>4</sub><sup>2-</sup> groups (Maslova et al., 2008; Sahu & Parida, 2002). The band at 438 cm<sup>-1</sup> is due to the P–O bending vibrations (Maslova



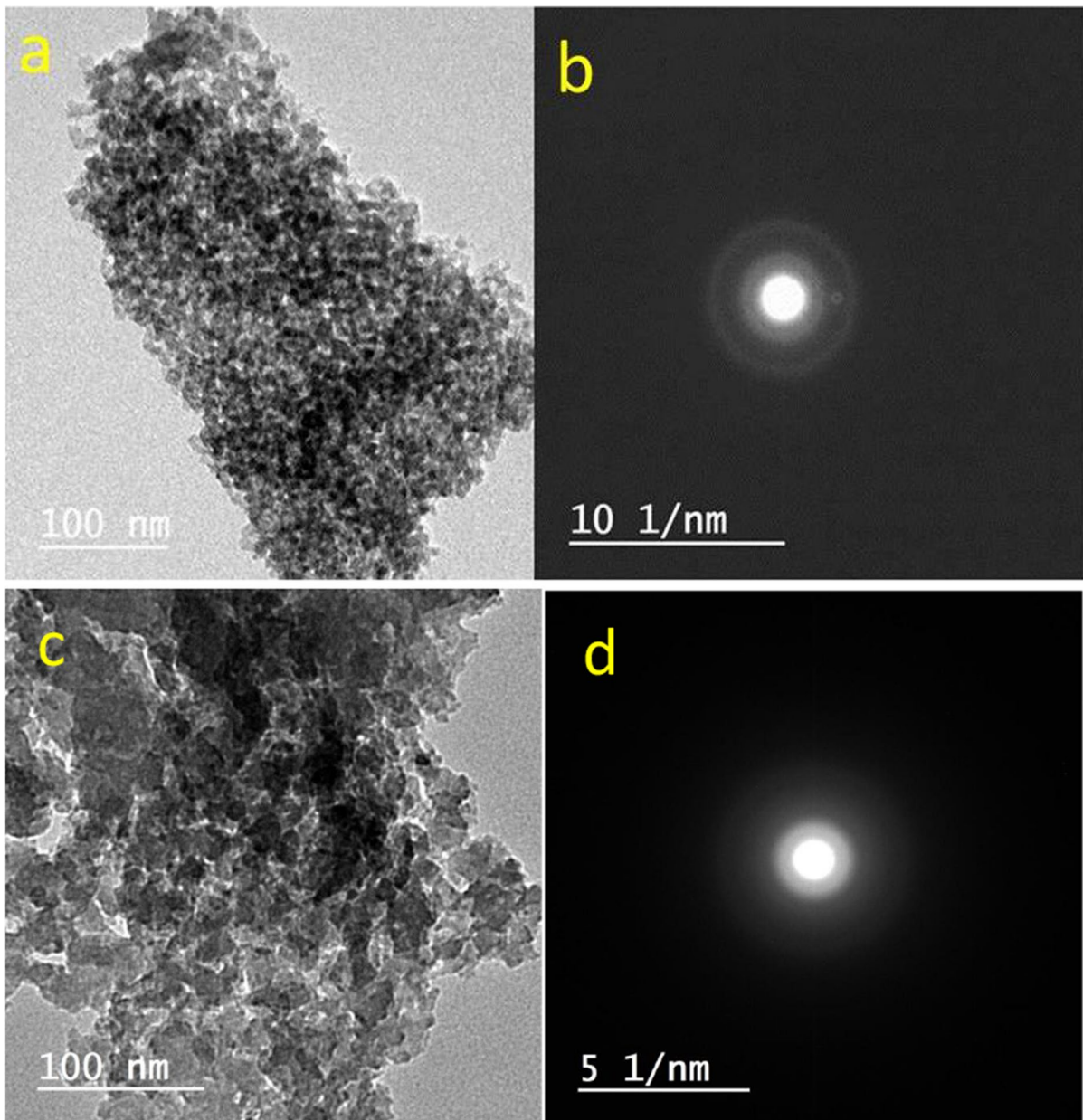
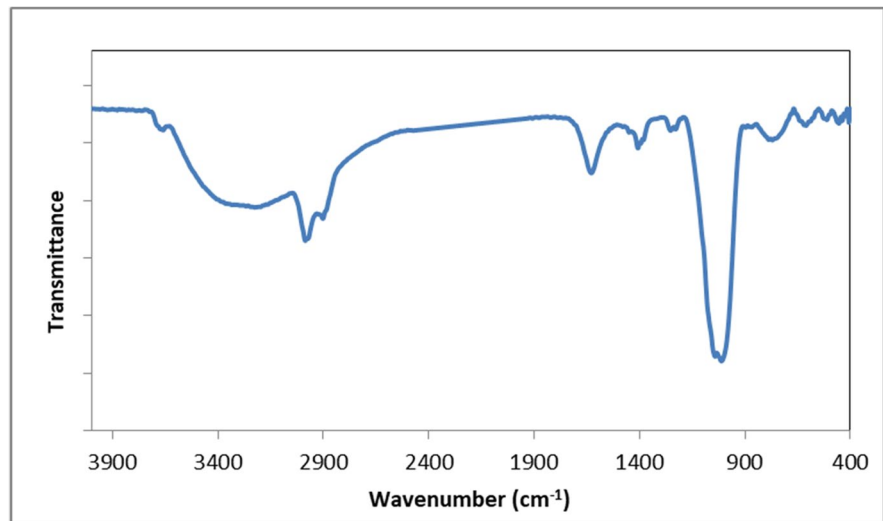


**Fig. 3** HRTEM images (a, c) and diffraction patterns (b, d) of the prepared TTP and TTPC samples, respectively

et al., 2008). The characteristic vibration peak at  $630\text{ cm}^{-1}$  is referred to Ti-O-P vibrations (Maslova et al., 2008). Besides, a vibration band at  $750\text{ cm}^{-1}$  appeared. This indicated the existence of nonbridging oxygen Ti-O bonds due to the presence of unreacted oxyhydroxide or terminal OH groups. Generally, the obtained characteristic peaks at  $1054$ ,  $630$  and  $438\text{ cm}^{-1}$  that referred to the bending and stretching

modes of Ti-O-P vibrations are substantially well-resolved. However, the OH- stretching vibrations of residual water around  $3400\text{ cm}^{-1}$  appeared broad and poor resolved. All of this data confirms the formation of titanium phosphate and suggests existence of OH groups connected to titanium (i.e., the formation of oxyhydroxide or hydroxyphosphate materials) (Maslova et al., 2008).

**Fig. 4** FTIR spectrum of TTP

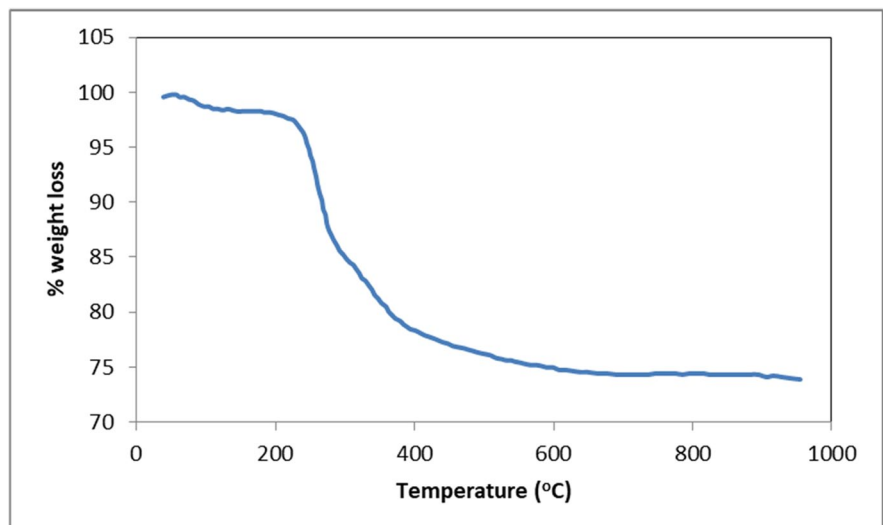


### 3.2.5 Thermogravimetric Analysis

The TGA data of TTP is depicted in Fig. 5. Data in Fig. 5 reveals the thermal decomposition of TTP in the temperature range of 75–1000 °C. The final product was a mixture of  $\text{TiO}_2$  and  $\text{Ti}_5\text{O}_4(\text{PO}_4)_4$  as confirmed by XRD. The total weight loss up to 700 °C was found to be 25.43% which is nearly similar to the estimated weight loss using XRF. TTP started to lose the adsorbed water at ~75–170 °C (weight loss =1.73%). When all of the physically adsorbed water was liberated, the composite decomposed above 200 °C. The first decomposition peak appeared at the

range 202–302 °C (weight loss =13.22%). At this range,  $\text{TiO}(\text{OH})_2$  started to lose its water molecules to form  $\text{TiO}_2$  (Yao et al., 2017). Besides, Ti-OH and phosphate groups simultaneously start to condense (Maslova et al., 2008). Further heating of TTP sample up to 1000 °C resulted in further weight loss (10.48%) until the formation of the end product which is a mixture of  $\text{TiO}_2$  and  $\text{Ti}_5\text{O}_4(\text{PO}_4)_4$  as confirmed by XRD. Combined with data obtained from XRD, the ratio of TTP constituents was calculated to be 38.38%  $\text{TiO}(\text{OH})_2$  and 59.89% titanium phosphate. Comparing the obtained data from TGA analysis with that previously presented in literature, one can conclude

**Fig. 5** TGA data of TTP under nitrogen atmosphere at a heating rate: 10 °C/min





that the structure of titanium phosphate in TTP contains only monohydrogenated phosphate group  $\text{HPO}_4^{2-}$ . Unlike titanium dihydrogen phosphate, the decomposition of titanium monohydrogen phosphate continued up to 700 °C occurring at two temperature ranges, which is similar to what TTP currently displayed (Maslova et al., 2008).

### 3.2.6 Surface Characterization

The nitrogen adsorption-desorption isotherms of TTP composites and pure carbon are depicted in Fig. 6a–d. In addition, Fig. 6e represents the pore volume distribution according to the NLDFT model. The surface textural properties are listed in Table 3. The values of the  $P/P^0$  at which the estimated total pore volumes were measured are also listed in Table 3. The surface parameters of TTP supported on activated carbon (TTPC) was also measured and compared with a physically mixed TTP with carbon (TPC(mix)) having the same TTP:C ratio (1:5). According to Brunauer's classification (Puma et al., 2008), the adsorption isotherm of TTP belongs to type II isotherm, having a gradual increase of  $\text{N}_2$ -adsorbed volume at high  $P/P^0$  region with a small hysteresis loop, indicating the presence of small amount of larger mesopores. However, the isotherms of C, TTPC, and TTPC (mix) belong to type I of Langmuir adsorption isotherm. All these carbonaceous samples displayed typical adsorption characteristic curves of the microporous structure. As indicated in Fig. 6b–d, the shape of the characteristic isotherm curve of carbon (C) did not exhibit significant change when TTP was loaded on its surfaces. This revealed the predominance of the microporous structure in TTPC and TTPC (mix) leading to the quick formation of  $\text{N}_2$  monolayer at low pressures.

As shown in Fig. 6e, the pore volume distribution indicates that TTP is a mesopores material while the carbonaceous samples are microporous materials according to the IUPAC classification. The pore width in TTP is ranging from 3.8 to 8 nm. However, the pore width of pure carbon and TTPC range from 0.4 to 2.8 and 0.4 to 2.6 nm, respectively.

As indicated in Table 3, the pure nano TTP has a relatively lower BET-specific surface area (143.8  $\text{m}^2/\text{g}$ ) comparing to the other TTP materials. However, it possesses the highest average pore size (6.7285 nm) and total pore volume (0.2419  $\text{cm}^3/\text{g}$ )

among the other investigated samples. Moreover, the specific surface area of C is slightly reduced from 1432.3 to 1294.9  $\text{m}^2/\text{g}$  by simple physical mixing with TTP. The mean pore diameter and total pore volume of C and TTPC (mix) are approximately the same. This is because the physical mixed loading method does not effectively disperse nano-TTP to the surface of carbon. Therefore, the retained large specific surface area is actually due to the surface of carbon. Contrary, the estimated surface parameters of TTPC revealed the significant decrease of surface area and total pore volume from 1432.3 to 550.8  $\text{m}^2/\text{g}$  and 0.5933 to 0.2353  $\text{cm}^3/\text{g}$ , respectively, upon loading of TTP on C via the simple precipitation method. This indicates that the loaded TTP successfully occupied the inner surfaces of C.

### 3.3 Batch Sorption Experiments

As previously illustrated, TTP materials were synthesized in acidic conditions. Thus, they were obtained in their proton forms. In this section, the sorption behavior of the proton form of TTP and TTPC were investigated for  $\text{Na}^+$  and  $\text{K}^+$  removal from water using batch experiments. TTP and TTPC were treated with either  $\text{NaNO}_3$  or  $\text{KNO}_3$  where the protons in the phosphate groups are exchanged with  $\text{Na}^+$  and  $\text{K}^+$  present in the solution. The initial pH values of Na and K nitrates' solutions were measured to be  $7 \pm 0.2$ .

As illustrated in Fig. 7, the removal of K and Na ions displayed slightly different behavior at different intervals of the reaction time. At the early 10 min, the removal of both cations using TTP occurred at rapid exchange rate. At this stage, the hydrogen ion exchange probably occurred via partial exchange of hydrogen ions in phosphate groups as well as through deprotonation of hydroxyl groups.

After 10 min., the exchange of both K and Na ions suddenly fall down followed by a second increase after 60 min. During the exchange reaction, the pH values drastically decreased due to the release of hydrogen ions. The final pH value of  $\text{KNO}_3$  solution was measured to be  $2.6 \pm 0.2$  and  $2.8 \pm 0.2$  using TTP. Desorption of some K and Na ions were observed after the first 10 min probably due to the re-protonation of hydroxyl groups at these low pH values. Further, as shown in Fig. 7,

**Fig. 6 a–d** Nitrogen adsorption-desorption isotherms of **a** TTP, **b** TTPC, **c** C, and **d** TTPC (mix), **e** pore volume distribution according to the NLDFT method

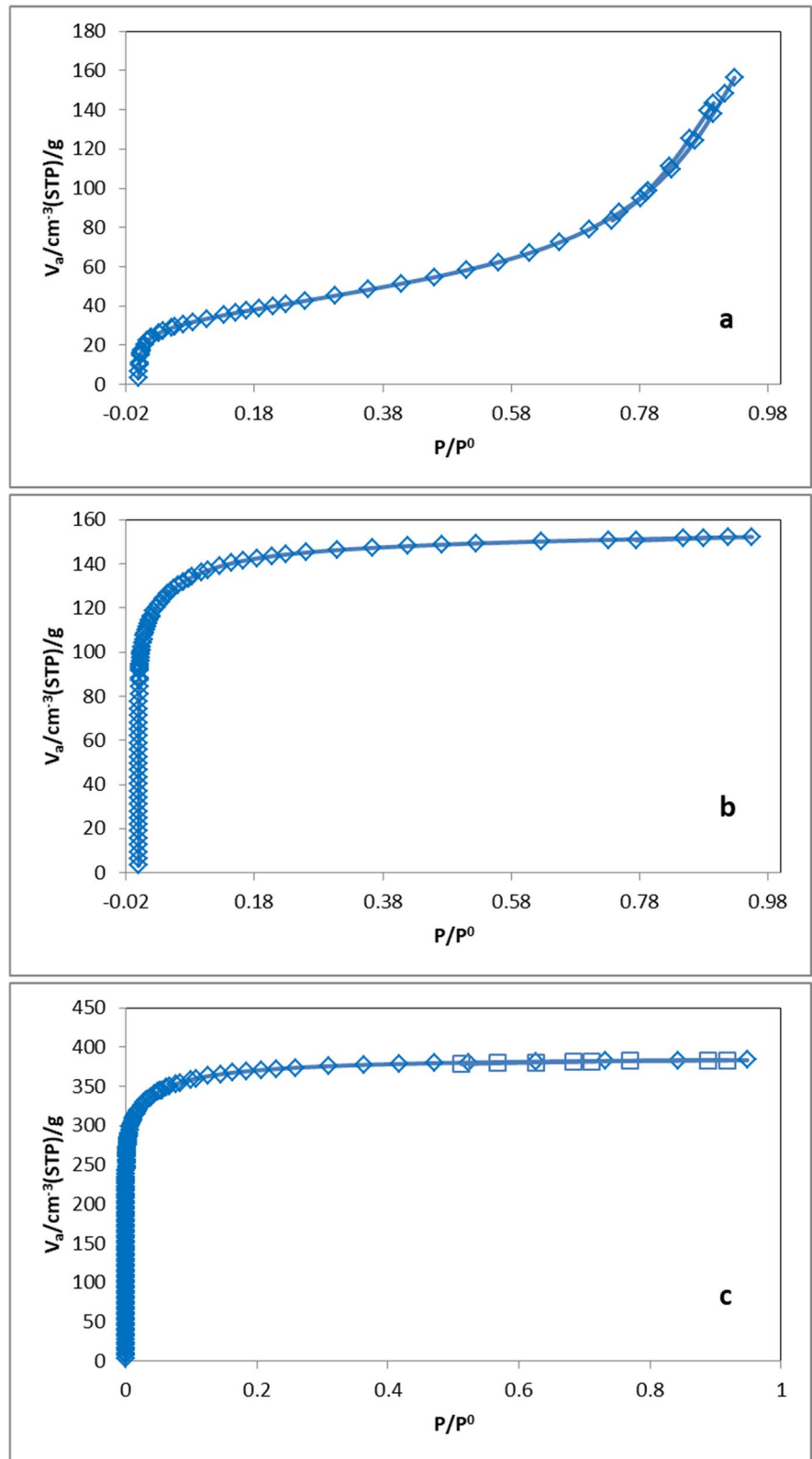
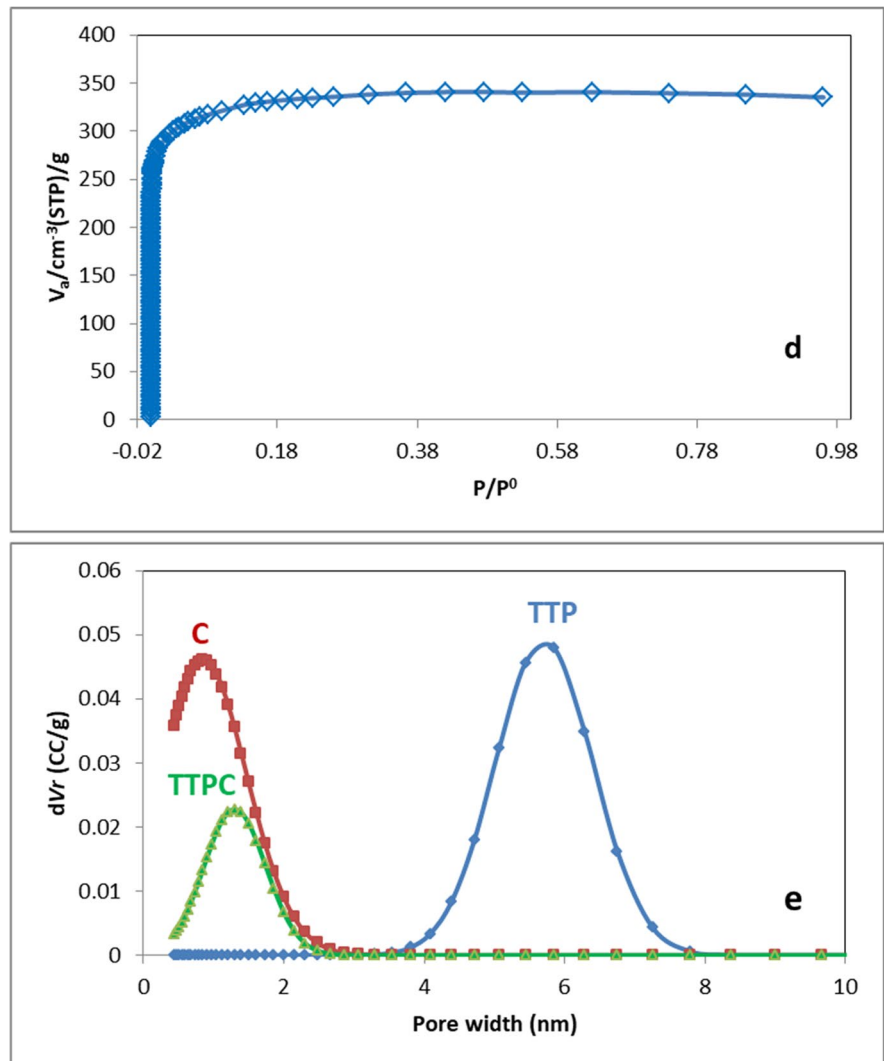


Fig. 6 (continued)



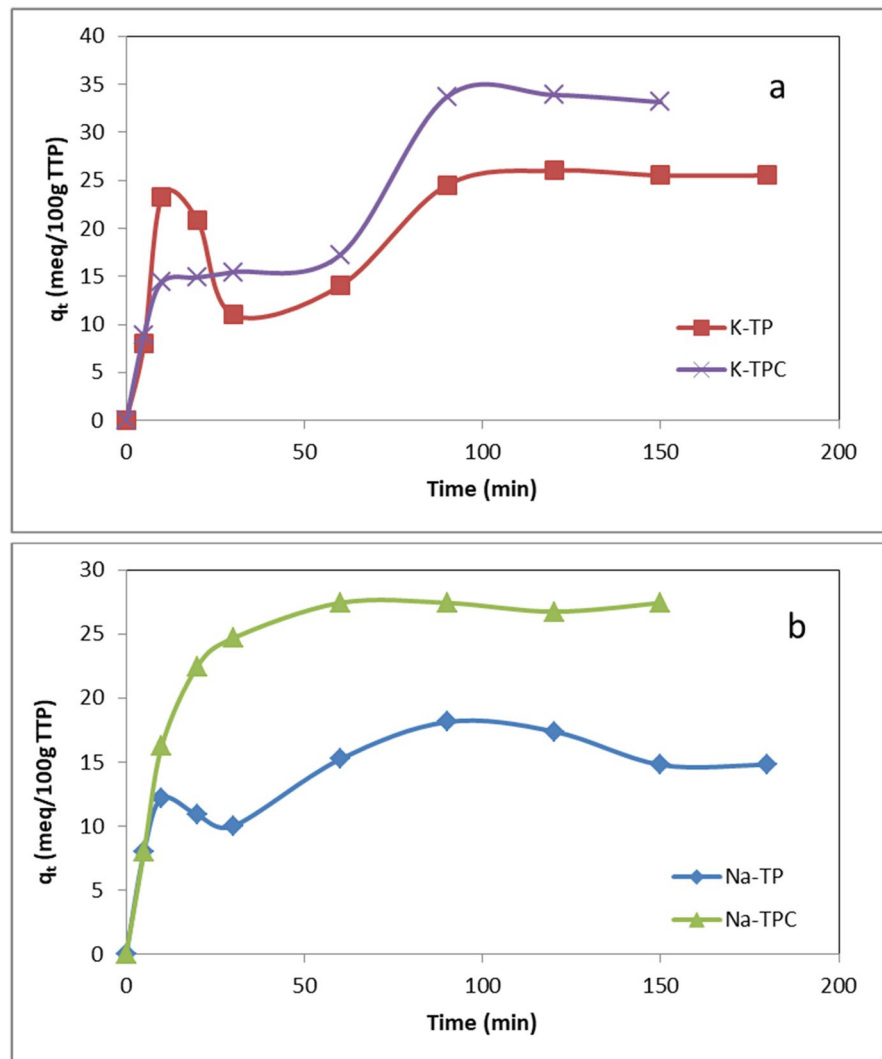
TTPC displayed higher affinity toward the removal of metal cations than that obtained by TTP. This revealed that supporting nano-TTP on activated carbon enhanced its removal efficiency.

**Table 3** The estimated surface parameters of the investigated samples

| Adsorbent | S <sub>BET</sub> (m <sup>2</sup> /g) | Mean pore diameter (nm) | Total pore volume (cm <sup>3</sup> /g) | P/P <sup>0</sup> (KPa) |
|-----------|--------------------------------------|-------------------------|--|------------------------|
| TTP       | 143.8                                | 6.7285                  | 0.2419                                 | 0.928                  |
| TTPC      | 550.8                                | 1.7087                  | 0.2353                                 | 0.955                  |
| C         | 1432.3                               | 1.6568                  | 0.5933                                 | 0.948                  |
| TTPC(mix) | 1294.9                               | 1.6022                  | 0.5184                                 | 0.960                  |

It is worth to mention that unlike K<sup>+</sup>, the removal of Na<sup>+</sup> ions constantly increased until they reach a plateau at longer reaction time (Fig. 7). The affinity of TTP toward K<sup>+</sup> removal was significantly higher than its affinity toward Na<sup>+</sup>. K<sup>+</sup> ions possess higher and mobility than that of Na<sup>+</sup> (Laidler and Meiser, 1982). The calculated Stokes radius of Na<sup>+</sup> is (1.94 Å) is larger than that of K<sup>+</sup> (1.34 Å) (Zhang et al., 2017). The large shell of water molecules that surround Na<sup>+</sup> ions significantly slowed down their diffusion toward TTP surfaces compared with K<sup>+</sup>. Therefore, K<sup>+</sup> ions diffused easier toward inner and outer surfaces of TTP. Thus, they more easily exchanged the H<sup>+</sup> ions. Consequently, the changes occurred due to the variation in the pH of

**Fig. 7** The effect of the reaction time on the removal of a:  $\text{Na}^+$  and b:  $\text{K}^+$  using TTP and TTPC



the reaction medium is more clearly observed in case of  $\text{K}^+$  ions removal.

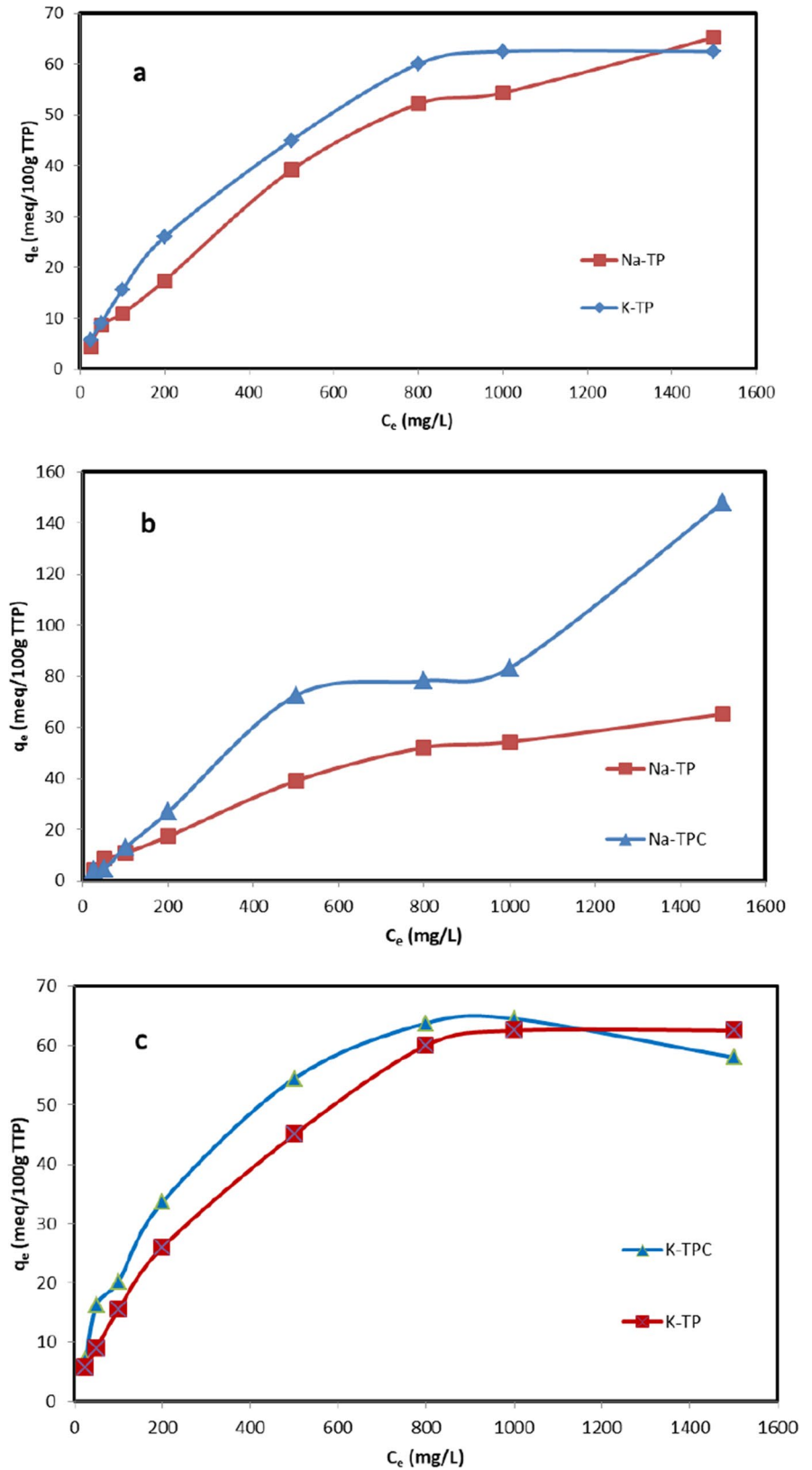
### 3.4 Sorption Isotherms

The amount of the sorbed cations on TTP and TTPC ( $q_e$ ) was significantly influenced by the initial concentration ( $C_0$ ) of  $\text{Na}^+$  and  $\text{K}^+$ . Figure 8a illustrates the relationship between  $q_e$  and  $C_0$  at the range (25–1500 mg/L) by using TTP. As shown in Fig. 8a, at relatively low initial concentrations (up to 1000 mg/L), the affinity of TTP toward  $\text{K}^+$  removal was significantly higher than its affinity toward  $\text{Na}^+$ . As previously mentioned,  $\text{K}^+$  ions possess higher mobility than that of  $\text{Na}^+$ . The large shell of water molecules

that surround  $\text{Na}^+$  ions significantly slow down their diffusion toward TTP surfaces compared with  $\text{K}^+$ . Therefore,  $\text{K}^+$  ions diffused easier toward inner and outer surfaces of TTP. Thus, they more easily exchanged the  $\text{H}^+$  ions.

On the other side, the sorption behavior of supported nano-TTP on activated carbon (TTPC) was investigated and compared to that of the unsupported TTP. Bare activated carbon showed no activity toward the removal of either  $\text{Na}^+$  or  $\text{K}^+$  ions. However, as shown in figures 8b and c, TTPC displayed higher affinity toward the removal of metal cations than that obtained by TTP. This revealed that supporting nano-TTP on activated carbon enhanced the removal efficiency of TTP. This observation is in agreement with

**Fig. 8** Change in the amount of  $K^+$  and  $Na^+$  ions removed by TTP and TPC composites at different initial concentrations





the data obtained by surface measurements. As previously discussed, the loaded nano-TTP in TPC was effectively dispersed inside the inner surfaces of C. Therefore, exposed surface area of supported nano-titanium phosphate in TTPC sample increased toward the targeted cations during the removal experiment.

Additionally, at high concentrations, the affinity of both TTP and TTPC toward the removal of  $K^+$  ions became nearly constant. Contrary, the removal of  $Na^+$  ions continuously increased at higher initial concentrations. At high initial concentrations, TTP material surfaces were surrounded by large number of hydrated sodium or potassium ions. The number of  $K^+$  ions is much higher than the number of  $Na^+$  ions per unit surface area of TTP. The large hydration shell surrounding  $Na^+$  ions, probably served to keep the  $Na^+$  ions more dispersed and separated. Therefore, the sorption of  $Na^+$  ions continued to increase at high initial concentrations. Meanwhile,  $K^+$  ions occupied the outer surface of TTP, blocking the entrance of the deeply inner pores and thus preventing further sorption.

Langmuir was selected as the adsorption model to study the stacking behavior of  $K^+$  and  $Na^+$  by TTP and TTPC as mentioned in section 2.

**Table 4** Langmuir sorption isotherm parameters of the Na and K ions removal by TTP samples

| Sample | Element | $q_m$ (meq/100g TTP) | $b$ (l/mg) | $R$    |
|--------|---------|----------------------|------------|--------|
| TTP    | Na      | 90.1                 | 0.00157    | 0.9747 |
| TTPC   | Na      | 188.7                | 0.0008     | 0.8995 |
| TTP    | K       | 81.97                | 0.0026     | 0.9929 |
| TTPC   | K       | 82.64                | 0.0038     | 0.9959 |

Applying Langmuir adsorption model on sorption batch data allows estimating the amount of metal ions that can be exchanged by TTP materials. The fitted constants for Langmuir model and their corresponding regression coefficients are summarized in Table 4. The maximum adsorption capacities ( $q_m$ ) derived from Langmuir plot were estimated to be 90.1, 188.7, 81.97, and 82.64 meq/100 g for Na-TP, Na-TPC, K-TP, and K-TPC, respectively.

### 3.5 The Effect of Initial pH of the Cation Solutions

The effect of the initial pH of K and Na ions solutions was investigated and illustrated in Fig. 9. Drops of diluted HCl and  $NH_4OH$  solutions were used to adjust the initial pH values. As seen in figure 9, the amount of the removed Na and K ions increased as the initial pH increased using both TTP and TTPC. However, remarkable decrease in the pH of the reaction media was observed at the end of the reaction media due to the release of the exchanged protons.

### 3.6 Determination of Ion-Exchange Capacity

The ion-exchange capacity of TTP was twice investigated through a simple acid-base back titration method by using either NaOH or KOH as indicated in the experimental section. The estimated exchange capacity values were found to be 10.60 and 11.55 meq/g TTP using NaOH and KOH, respectively. The obtained values revealed that the maximal affinity of TTP to exchange  $K^+$  is slightly higher than  $Na^+$  ions under the given experimental conditions. The removal of both K and Na ions is drastically higher than those previously estimated by using sodium and potassium nitrates even at high initial pH values. Herein, sodium

**Fig. 9** The effect of pH on Na and K ions removal by TTP and TTPC

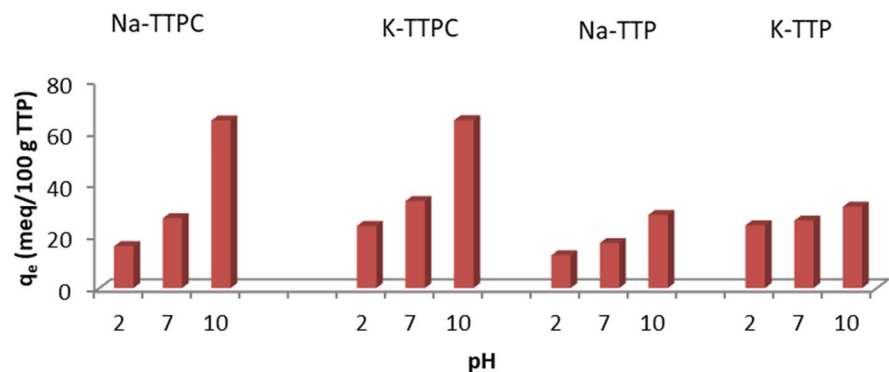


**Table 5** Exchange capacities of titanium phosphate materials using the back titration method

| Exchange capacity <i>E</i><br>(in mg-eq g <sup>-1</sup> ) | Reference              |
|---|------------------------|
| Up to 3.8   | (Maslova et al., 2012) |
| 5.56  | (Maslova et al., 2013) |
| 10.6  | Current work           |

**Table 6** Preliminarily chemical analyses of the collected samples from Rahawy drain at rush hour (at 12:00)

| Parameter               | Sample 1 | Sample 2 | Sample 3 |
|-------------------------|----------|----------|----------|
| EC US/cm                | 1.875    | 1.075    | 1.138    |
| pH                      | 7.43     | 8.7      | 7.33     |
| TDS (mg/l)              | 1200     | 692      | 728      |
| Ca <sup>++</sup> (mg/l) | 82.76    | 71.38    | 51.56    |
| Mg <sup>++</sup> (mg/l) | 31.29    | 8.94     | 23.91    |
| Na <sup>+</sup> (mg/l)  | 278      | 91.5     | 120      |
| K <sup>+</sup> (mg/l)   | 21       | 11.9     | 18       |

and potassium hydroxides kept the pH of the reaction media high during the removal experiments. At high pH values, all exchangeable protons in the hydrogen

titanium phosphate and titanium oxyhydroxide participated in the removal processes. Combining the data obtained from TGA, XRD, XRF, and the exchange capacity experiments, the theoretical exchange capacities of the individual parts of TTP are estimated to be 7.68 and 3.83 meq/g TTP for titanium oxyhydroxide and hydrogen titanium phosphate, respectively.

Additionally, the obtained exchange capacity of TTP composite toward Na ions is significantly higher when compared to some of the previously reported pure titanium phosphate materials in literature using the same back titration method as illustrated in Table 5. Data in Table 5 reveals the potential outstanding performance of our TTP composites against the removal of ions particularly from the basic sodic waters.

### 3.7 Real Wastewater Treatment

In this work, the remediation of highly polluted real wastewater from EL-Rahawy drain by TTP and TTPC composites were investigated. Preliminary chemical analyses of collected wastewater samples from EL-Rahawy drain are illustrated in Table 6. Further, Table 7 provides full analysis of the collected real wastewater sample to be treated by TTP materials. As seen in Tables 6 and 7, the waters contained relatively

**Table 7** Full analysis of the real wastewater collected from Rahawy drain before and after the treatment using TTP and TTPC

| Parameter               | Rahawy drain | Rahawy drain after treatment with TTP | Rahawy drain after treatment with TTPC |
|-------------------------|--------------|---------------------------------------|--|
| COD (mg/l)              | 202          | 28.6                                  | 16.3                                   |
| EC US/cm                | 1.825        | 1.082                                 | 1.467                                  |
| pH                      | 7.67         | 5.29                                  | 4.03                                   |
| TDS (mg/l)              | 1168         | 692                                   | 938                                    |
| Ca <sup>++</sup> (mg/l) | 111.15       | 7.21                                  | 0.6                                    |
| Mg <sup>++</sup> (mg/l) | 28.09        | 11.42                                 | 29.88                                  |
| Na <sup>+</sup> (mg/l)  | 174          | 125                                   | 142                                    |
| K <sup>+</sup> (mg/l)   | 16.76        | 2.66                                  | 9.24                                   |
| NH <sub>3</sub> (mg/l)  | 32           | 5.3                                   | 11.8                                   |
| Barium (mg/l)           | 0.053        | < 0.005                               | < 0.005                                |
| Cadmium (mg/l)          | 0.044        | 0.006                                 | 0.002                                  |
| Cobalt (mg/l)           | 0.0275       | 0.0169                                | 0.0174                                 |
| Copper (mg/l)           | 0.0153       | < 0.006                               | < 0.006                                |
| Iron (mg/l)             | 1.99         | 0.6831                                | 0.6148                                 |
| Manganese (mg/l)        | 0.4424       | 0.0359                                | 0.2139                                 |
| Zinc (mg/l)             | 0.2422       | 0.0124                                | 0.0567                                 |

significant amount of sodium, potassium, toxic heavy metals, and organic pollutants. The pH values of the collected samples are slightly high which is adequate for the better performance of TTP materials.

Thus, the treatment of the polluted wastewater was investigated by using TTP materials (w/v=1:100). Two sorption experiments were conducted using TTP and TTPC as the target sorbents. As shown in Table 7, the amount of K ions was decreased by 84.13% and 44.8% by using 1 g of TTP and TPC, respectively. Meanwhile, the amount of Na ions was decreased by 28.6% and 18.4% by using TTP and TPC, respectively.

Table 7 also revealed significant decrease in the levels of other different metal cations, total dissolved solids (TDS) and even organic contaminants represented by the chemical oxygen demand (COD) was obtained upon using any of these composites. Based on the given data, one can conclude that the remediation of highly polluted real wastewater from EL-Rahawy drain by TTP and TTPC composites were successfully achieved.

## 4 Conclusion

Titanium oxyhydroxide/titanium phosphate (TTP) and TTP-active carbon (TTPC) composites have been successfully prepared under mild conditions. XRD, HRTEM, XRF, TGA, and FTIR revealed the formation of nano-sized low crystalline material (average diameter of TTP ~ 6 nm) composed of 38.38%  $\text{TiO}(\text{OH})_2$  and 59.89% titanium phosphate. The structure of titanium phosphate in TTP most probably contains only monohydrogenated phosphate group  $\text{HPO}_4^{2-}$ . The surface properties of TTP and TTPC were measured and compared with a physically mixed TTP with carbon. The pure nano TTP has a relatively lower BET-specific surface area ( $143.8 \text{ m}^2/\text{g}$ ) comparing to the other TTP materials. However, TTP possesses the highest average pore size ( $6.7285 \text{ nm}$ ) and total pore volume ( $0.2419 \text{ cm}^3/\text{g}$ ) among the other investigated samples. Significant decrease of surface area and total pore volume of active carbon from  $1432.3$  to  $550.8 \text{ m}^2/\text{g}$  and  $0.5933$  to  $0.2353 \text{ cm}^3/\text{g}$ , respectively was observed upon loading of TTP on active carbon (C) indicating the successful inclusion of TTP within the inner surfaces of C. TTP and TTPC displayed different removal behavior against

Na and K ions. The maximum adsorption capacities derived from Langmuir plot were estimated to be 90.1, 188.7, 81.97, and 82.64 meq/100g for Na-TP, Na-TPC, K-TP, and K-TPC, respectively. The maximal removal capacities of TTP were achieved in the highly basic waters. They were measured to be 10.60 and 11.55 meq/g TTP with respect to Na and K ions, respectively. At high pH values, all exchangeable protons in the hydrogen titanium phosphate and titanium oxyhydroxide participated in the removal processes. The removal capacities of the individual parts of TTP are estimated to be 7.68 and 3.83 meq/g for titanium oxyhydroxide and hydrogen titanium phosphate, respectively. Remediation of highly polluted real wastewater from EL-Rahawy drain by TTP and TTPC composites were successfully achieved. The full analysis of the treated real wastewater revealed significant decrease in the levels of metal cations, total dissolved solids (TDS), and even organic contaminants represented by the chemical oxygen demand (COD) was obtained upon using any of these composites.

**Funding** Open access funding provided by The Science, Technology & Innovation Funding Authority (STDF) in cooperation with The Egyptian Knowledge Bank (EKB).

**Data Availability** The data used to support the findings of this study are included within the article.

## Declarations

**Conflict of Interest** The authors declare no competing interests.

**Open Access** This article is licensed under a Creative Commons Attribution 4.0 International License, which permits use, sharing, adaptation, distribution and reproduction in any medium or format, as long as you give appropriate credit to the original author(s) and the source, provide a link to the Creative Commons licence, and indicate if changes were made. The images or other third party material in this article are included in the article's Creative Commons licence, unless indicated otherwise in a credit line to the material. If material is not included in the article's Creative Commons licence and your intended use is not permitted by statutory regulation or exceeds the permitted use, you will need to obtain permission directly from the copyright holder. To view a copy of this licence, visit <http://creativecommons.org/licenses/by/4.0/>.

## References

Ahn, M.-S., Ahmad, R., Yoo, J.-Y., & Hahn, Y.-B. (2018). Synthesis of manganese oxide nanorods and its application for

- potassium ion sensing in water. *Journal of Colloid and Interface Science*, 516, 364–370. <https://doi.org/10.1016/j.jcis.2018.01.081>
- Alberti, G., Casciola, M., Costantino, U., & Vivani, R. (1996). Layered and pillared metal (IV) phosphates and phosphonates. *Advanced Materials*, 8, 291–303. <https://doi.org/10.1002/adma.19960080405>
- American Public Health Association “APHA” method (2017). Standard methods for the examination of water and wastewater, (23th Edition).
- Björklund, K., & Li, L. Y. (2017). Adsorption of organic stormwater pollutants onto activated carbon from sewage sludge. *Journal of Environmental Management*, 197, 490–497. <https://doi.org/10.1016/j.jenvman.2017.04.011>
- Bortun, A., Jaimez, E., Llavona, R., García, J., & Rodríguez, J. (1995). Formation of crystalline titanium(IV) phosphates from titanium(III) solutions. *Material Research Bulletin*, 30(4), 413–420. [https://doi.org/10.1016/0025-5408\(95\)00019-4](https://doi.org/10.1016/0025-5408(95)00019-4)
- Botomé, M. L., Poletto, P., Junges, J., Perondi, D., Dettmer, A., & Godinho, M. (2017). Preparation and characterization of a metal-rich activated carbon from CCA-treated wood for CO<sub>2</sub> capture. *Chemical Engineering Journal*, 321, 614–621. <https://doi.org/10.1016/j.cej.2017.04.004>
- Bruque, S., Aranda, M. A. G., Losilla, E. R., Olivera-Pastor, P., & Maireles-Torres, P. (1995). Synthesis optimization and crystal structures of layered metal(IV) hydrogen phosphates,  $\alpha$ -M(HPO<sub>4</sub>)<sub>2</sub>·H<sub>2</sub>O (M = Ti, Sn, Pb). *Inorganic Chemistry*, 34(4), 893–899. <https://doi.org/10.1039/c5dt02648b>
- EL-Mekkawi, D. M., Abdelwahab, N. A., Mohamed, W. A., Taha, N. A., & Abdel-Mottaleb, M. S. A. (2020). Solar photocatalytic treatment of industrial wastewater utilizing recycled polymeric disposals as TiO<sub>2</sub> supports. *Journal of Cleaner Production*, 249, 119430. <https://doi.org/10.1016/j.jclepro.2019.119430>
- EL-Mekkawi, D. M., Galal, H. R., Abd EL Wahab, R. M., & Mohamed, W. A. A. (2016). Photocatalytic activity evaluation of TiO<sub>2</sub> nanoparticles based on COD analyses for water treatment applications: A standardization attempt. *International Journal of Environmental Science and Technology*, 13, 1077–1088. <https://doi.org/10.1007/s13762-016-0944-0>
- EL-Mekkawi, D. M., Ibrahim, F. A., & Selim, M. M. (2016). Removal of methylene blue from water using zeolites prepared from Egyptian kaolins collected from different sources. *Journal of Environmental Chemical Engineering*, 4, 1417–1422. <https://doi.org/10.1016/j.jece.2016.01.007>
- EL-Mekkawi, D. M., & Selim, M. M. (2014). Removal of Pb<sup>2+</sup> from water by using Na-Y zeolites prepared from Egyptian kaolins collected from different sources. *Journal of Environmental Chemical Engineering*, 2, 723–730. <https://doi.org/10.1016/j.jece.2013.11.014>
- Filipe-Ribeiro, L., Milheiro, J., Matos, C. C., Cosme, F., & Nunes, F. M. (2017). Data on changes in red wine phenolic compounds, headspace aroma compounds and sensory profile after treatment of red wines with activated carbons with different physicochemical characteristics. *Data Brief*, 12, 188–202. <https://doi.org/10.1016/j.foodchem.2017.02.066>
- Guo, S.-Y., & Han, S. (2014). Constructing a novel hierarchical 3D flower-like nano/micro titanium phosphate with efficient hydrogen evolution from water splitting. *Journal of Power Sources*, 267, 9–13. <https://doi.org/10.1016/j.jpowsour.2014.05.011>
- Guo, S.-Y., Han, S., Chi, B., Pu, J., & Li, J. (2014). Synthesis of shape-controlled mesoporous titanium phosphate nanocrystals: The hexagonal titanium phosphate with enhanced hydrogen generation from water splitting. *International Journal of Hydrogen Energy*, 39, 2446–2453. <https://doi.org/10.1016/j.ijhydene.2013.12.007>
- Ibrahim, A. M., El-Mekkawi, D. M., & Selim, M. M. (2020). Supported TiO<sub>2</sub> on kaolin, cordierite and calcite for photocatalytic removal of dyes from wastewater. *CLEAN – Soil, Air, Water*, 48, 1900361. <https://doi.org/10.1002/clean.201900361>
- Janusz, W., Khalameida, S., Skwarek, E., Skubiszewska-Zieba, J., Sydoruk, V., & Charnas, B. (2019). Modification of titanium phosphate precipitated from titanysulfate. *Journal of Thermal Analysis and Calorimetry*, 135, 2925–2934. <https://doi.org/10.1007/s10973-018-7611-2>
- Laidler, K. J., & Meiser, J. H. (1982). *Physical chemistry, Benjamin/Cummings* (p. 274).
- Langmuir, I. (1918). The adsorption of gases on plane surfaces of glass, mica and platinum. *Journal of the American Chemical Society*, 40, 1361–1403. <https://doi.org/10.1021/ja02242a004>
- Liu, J., Wei, X., Yu, Y., Song, J., Wang, X., Li, A., Liu, X.-W., & Deng, W.-Q. (2010). Uniform core-shell titanium phosphate nanospheres with orderly open nanopores: A highly active Brønsted acid catalyst. *Chemical Communication*, 46, 1670–1672. <https://doi.org/10.1039/B922100J>
- Maslova, M. V., Chugunov, A. S., Gerasimova, L. G., & Konovalova, N. V. (2013). Acidbase and sorption properties of amorphous titanium phosphate. *Radiochemistry*, 55(4), 392–398.
- Maslova, M. V., Rusanova, D., Naydenov, V., Antzutkin, O. N., & Gerasimova, L. G. (2008). Synthesis, characterization, and sorption properties of amorphous titanium phosphate and silica-modified titanium phosphates. *Inorganic Chemistry*, 47, 11351–11360. <https://doi.org/10.1021/ic801274z>
- Maslova, M. V., Rusanova, D., Naydenov, V., Antzutkin, O. N., & Gerasimova, L. G. (2012). Extended study on the synthesis of amorphous titanium phosphates with tailored sorption properties. *Journal of Non-Crystalline Solids*, 358, 2943–2950. <https://doi.org/10.1016/j.jnoncrysol.2012.06.033>
- Maslova, M. V., Rusanova, D., Naydenov, V., Antzutkin, O. N., & Gerasimova, L. G. (2018). A new microporous oxyfluorinated titanium(IV) phosphate as an efficient heterogeneous catalyst for the selective oxidation of cyclohexanone. *Journal of Colloid and Interface Science*, 511, 92–100. <https://doi.org/10.1016/j.jcis.2017.09.115>
- Onoda, H., Fujikado, S., & Toyama, T. (2014). Preparation of titanium phosphate white pigments with titanium sulfate and their powder properties. *Journal of Advanced Ceramics*, 3(2), 132–136. <https://doi.org/10.1007/s40145-014-0103-3>
- Onoda, H., & Yamaguchi, T. (2012a). Synthesis of titanium phosphates with additives and their powder properties for

- cosmetics. *Materials Sciences and Applications*, 3, 18–23. <https://doi.org/10.4236/msa.2012.31003>
- Onoda, H., & Yamaguchi, T. (2012b). Influence of ultrasonic treatment on preparation and powder properties of titanium phosphates. *Journal of Materials Chemistry*, 22(37), 19826–19830. <https://doi.org/10.1039/C2JM33952H>
- Onoda, H., Yamaguchi, T., & Takenaka, A. (2021). Synthesis and pigmental properties of titanium phosphates with the addition of urea. *International Journal of Cosmetic Science*, 34, 86–90. <https://doi.org/10.1111/j.1468-2494.2011.00685.x>
- Puma, G. L., Bono, A., Krishnaiah, D., & Collin, J. G. (2008). Preparation of titanium dioxide photocatalyst loaded onto activated carbon support using chemical vapor deposition: a review paper. *Journal of Hazardous Materials*, 157, 209–219. <https://doi.org/10.1016/j.jhazmat.2008.01.040>
- Qureshi, M., & Varshney, K. G. (1991). *Inorganic ion exchangers in chemical analysis*. Taylor & Francis. <https://doi.org/10.1201/9780203750780>
- Sahu, B. B., & Parida, K. (2002). Cation exchange and sorption properties of crystalline  $\alpha$ -titanium (IV) phosphate. *Journal of Colloid and Interface Science*, 248, 221–230. <https://doi.org/10.1006/jcis.2001.7818>
- Sebastian, A., Nangia, A., & Prasad, M. N. V. (2019). Cadmium and sodium adsorption properties of magnetite nanoparticles synthesized from Hevea brasiliensis Muell. Arg. bark: Relevance in amelioration of metal stress in rice. *Journal of Hazardous Materials*, 371, 261–272. <https://doi.org/10.1016/j.jhazmat.2019.03.021>
- Selim, M. M., EL-Mekkawi, D. M., Aboelenin, R. M. M., Sayed, A. S. A., & Mohamed, G. M. (2017). Preparation and characterization of Na-A zeolite from aluminum scrub and commercial sodium silicate for the removal of  $\text{Cd}^{2+}$  from water. *Journal of the Association of Arab Universities for Basic and Applied Sciences*, 24, 19–25. <https://doi.org/10.1016/j.jaubas.2017.05.002>
- Serre, C., Taulelle, F., & Ferey, G. (2012). Rational design of porous titanophosphates. *Chemical Communication*, 2003(22), 2755–2765. <https://doi.org/10.1039/B304703B>
- Suhas, P. J. M., Carrott, M. M. L., Carrott, R., Singh, R., Singh, L. P., & Chaudhary, M. (2017). An innovative approach to develop microporous activated carbons in oxidising atmosphere. *Journal of Cleaner Production*, 156, 549–555. <https://doi.org/10.1016/j.jclepro.2017.04.078>
- Tegehall, P.-E. (1986). Synthesis of crystalline titanium(IV) phosphates by direct precipitation from Ti(III) solutions and ion exchange properties of some of the prepared phases. *Acta Chemica Scandinavica*, 40a, 507–514. <https://doi.org/10.3891/acta.chem.scand.40a-0507>
- Trublet, M., Maslova, M. V., Rusanova, D., & Antzutkin, O. N. (2016). Mild syntheses and surface characterization of amorphous  $\text{TiO}(\text{OH})\text{-(H}_2\text{PO}_4\text{)-H}_2\text{O}$  ion-exchanger. *Materials Chemistry and Physics*, 183, 467–475. <https://doi.org/10.1016/j.matchemphys.2016.09.002>
- Velo-Gala, I., Lopez-Penalver, J. J., Sánchez-Polo, M., & Rivera-Utrilla, J. (2017). Role of activated carbon surface chemistry in its photocatalytic activity and the generation of oxidant radicals under UV or solar radiation. *Applied Catalysis B*, 207, 412–423. <https://doi.org/10.1016/j.apcatb.2017.02.028>
- Yao, H., Toan, S., Huang, L., Fan, M., Wang, Y., Russell, A. G., Luo, G., & Fei, W. (2017).  $\text{TiO}(\text{OH})_2$  – highly effective catalysts for optimizing  $\text{CO}_2$  desorption kinetics reducing  $\text{CO}_2$  capture cost: A new pathway. *Scientific Reports*, 7, 2943. <https://doi.org/10.1038/s41598-017-03125-w>
- Zhang, Q., Chen, H., Wu, T., Jin, T., Pan, Z., Zheng, J., Gao, Y., & Zhuang, W. (2017). The opposite effects of sodium and potassium cations on water dynamics. *Chemical Science*, 8(2), 1429–1435. <https://doi.org/10.1039/c6sc03320b>
- Zhang, W., Koivula, R., Wiikinkoski, E., Xu, J., Hietala, S., Lehto, J., & Harjula, R. (2017). Efficient and selective recovery of trace scandium by inorganic titanium phosphate ion-exchangers from leachates of waste bauxite residue. *ACS Sustainable Chemistry & Engineering*, 5, 3103–3114. <https://doi.org/10.1021/acssuschemeng.6b02870>
- Zhang, X., Gu, P., Li, X., & Zhang, G. (2017). Efficient adsorption of radioactive iodide ion from simulated wastewater by nano  $\text{Cu}_2\text{O}/\text{Cu}$  modified activated carbon. *Chemical Engineering Journal*, 322, 129–139. <https://doi.org/10.1016/j.cej.2017.03.102>

**Publisher's Note** Springer Nature remains neutral with regard to jurisdictional claims in published maps and institutional affiliations.